TISSUE ENGINEERING
Volume 11, Number 9/10, 2005

Polymer Scaffolds Fabricated with Pore-Size Gradients as a Model for Studying the Zonal Organization within Tissue-Engineered Cartilage Constructs

T.B.F. WOODFIELD,[1,2] C.A. VAN BLITTERSWIJK, Ph.D.,[1] J. DE WIJN, Ph.D.,[2] T.J. SIMS, Ph.D.,[3] A.P. HOLLANDER, Ph.D.,[3] and J. RIESLE, Ph.D.[1,4]

ABSTRACT

The zonal organization of cells and extracellular matrix (ECM) constituents within articular cartilage is important for its biomechanical function in diarthroidal joints. Tissue-engineering strategies adopting porous three-dimensional (3D) scaffolds offer significant promise for the repair of articular cartilage defects, yet few approaches have accounted for the zonal structural organization as in native articular cartilage. In this study, the ability of anisotropic pore architectures to influence the zonal organization of chondrocytes and ECM components was investigated. Using a novel 3D fiber deposition (3DF) technique, we designed and produced 100% interconnecting scaffolds containing either homogeneously spaced pores (fiber spacing, 1 mm; pore size, about 680 μm in diameter) or pore-size gradients (fiber spacing, 0.5–2.0 mm; pore size range, about 200–1650 μm in diameter), but with similar overall porosity (about 80%) and volume fraction available for cell attachment and ECM formation. *In vitro* cell seeding showed that pore-size gradients promoted anisotropic cell distribution like that in the superficial, middle, and lower zones of immature bovine articular cartilage, irrespective of dynamic or static seeding methods. There was a direct correlation between zonal scaffold volume fraction and both DNA and glycosaminoglycan (GAG) content. Prolonged tissue culture *in vitro* showed similar inhomogeneous distributions of zonal GAG and collagen type II accumulation but not of GAG:DNA content, and levels were an order of magnitude less than in native cartilage. In this model system, we illustrated how scaffold design and novel processing techniques can be used to develop anisotropic pore architectures for instructing zonal cell and tissue distribution in tissue-engineered cartilage constructs.

INTRODUCTION

IT IS WELL ESTABLISHED that the regenerative capacity of damaged or diseased articular cartilage is limited.[1,2] Numerous strategies have been employed to deliver or recruit reparative cells to defects, with or without a three-dimensional (3D) scaffold, for the express purpose of production and organization of extracellular matrix (ECM) components.[3,4] It has been noted, however, that virtually none of these cell- or scaffold-based cartilage repair strategies employed to date accounts for the high degree of topographical organization of cells and ECM constituents within native hyaline cartilage.[1,3]

Chondrocytes are responsible for the synthesis and maintenance of articular cartilage, and yet occupy only a small portion (typically less than 2%) of the total volume

[1]Institute for Biomedical Technology, University of Twente, Enschede, The Netherlands.
[2]Centre for Bioengineering, University of Canterbury, Christchurch, New Zealand.
[3]Department of Rheumatology, University of Bristol, Bristol, United Kingdom.
[4]Cell Co Tec B.V., Bilthoven, The Netherlands.

of adult tissue[5] compared with the remaining interstitial water (about 80%) and ECM components (about 20%), such as type II collagen, noncollagenous proteins, and a high concentration of cartilage proteoglycans.[6,7] Mature chondrocytes are well differentiated in their lineage and the ECM in which they assemble has a highly organized internal structure.[5,7] Distinct variations in cell density and morphology, collagen fibril diameter and orientation, water concentration, and glycosaminoglycan (GAG) concentration exist with depth from the articular surface[5,6,8] and can be divided into four zones: the superficial, middle, and deep zones, and the zone of calcified cartilage, as illustrated in Fig. 1A. The superficial (*S*) zone contains flattened chondrocytes and densely packed collagen fibrils (diameter, 20 nm) oriented tangentially to the articular surface. The middle (*M*) zone contains randomly oriented collagen fibers and more rounded chondrocytes, whereas the lower (*L*), or deep, zone consists of large, spherical chondrocytes aligned in a columnar fashion, and thicker collagen fibers (diameter, 120 nm) oriented perpendicular to the joint surface. Chondrocytes isolated from these superficial, middle, and deep zones have been shown to exhibit different metabolic activities,[9] and in 3D culture experiments maintain their ability to synthesize ECM components specific to their zonal origin.[10,11]

The complex zonal organization and interaction between solid ECM and fluid components within articular cartilage are directly related to its biomechanical function.[12,13] It provides the tissue with near frictionless articulation and remarkable load-bearing abilities due to its viscoelastic behavior, as well as zone- and frequency-dependant stiffness under mechanical compression.[14–17] The inexorable functional demands necessary in load-bearing cartilage may require the repair tissue to closely resemble that of native tissue in terms of composition and organization for long-term success.[3,13] Because chon-

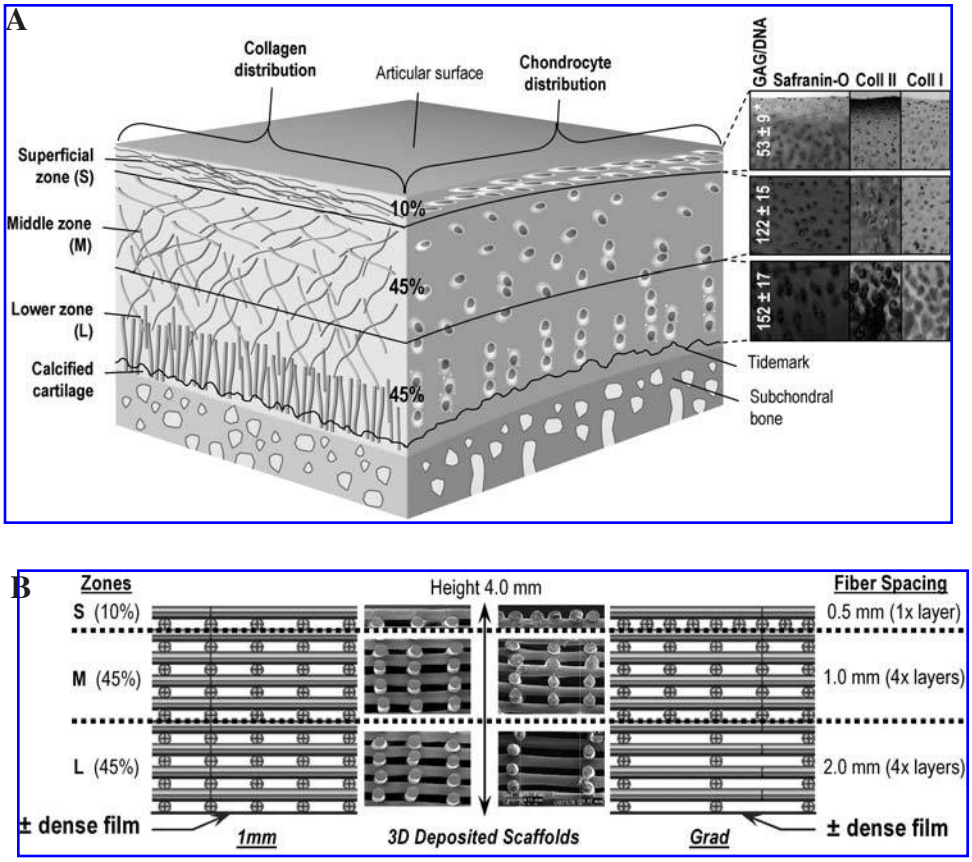

FIG. 1. (**A**) Anisotropic distribution and orientation of collagen fibers (*left face*) and chondrocytes (*right face*) within the superficial (*S*, 10%), middle (*M*, 45%), and deep or lower (*L*, 45%) zones of articular cartilage. GAG:DNA content, safranin O staining for GAG, and immunohistochemistry for collagen type II and type I of bovine articular cartilage are illustrated at right (*significant decrease in GAG:DNA content). (**B**) Corresponding zonal design and SEM pictures of model 3D-deposited scaffolds containing either a homogeneous 1-mm fiber spacing (*1mm*) or an anisotropic pore-size gradient (*Grad*). Regions corresponding to the upper (*S* – 10%), middle (*M* – 45%), and lower zones (*L* – 45%) are indicated on the *left*, whereas the associated fiber spacing used in *Grad* scaffolds (0.5, 1.0, and 2.0 mm) are indicated on the *right*. The same architectures were used to construct *1mmF* and *GradF* scaffolds on a basal dense film (50 μm thick).

drocytes are responsible for synthesis of cartilage ECM, the hypothesis is that by imitating the zonal organization within native tissue, the local cell environment will also stimulate synthesis of an organized cartilage construct.

As a step in this direction, studies have investigated the possibility of incorporating biological recognition or "instructive" features into biomaterial implants.[18,19] With respect to cartilage tissue engineering, polymer scaffolds with cell-excluding barriers or vertically oriented pores or channels have been developed,[20–22] as have seeding methods using cells suspended in photopolymerizing hydrogels,[10,23] agarose,[24] or alginate.[25] Moreover, instead of using a heterogeneous mixture of cells isolated from full-thickness cartilage, these studies in gels typically involved separate expansion and/or culture of zonal cell populations, isolated from the superficial, middle, and deep zone cartilage, and have assisted in tailoring an anisotropic cell distribution or tissue exhibiting specific superficial zone proteins.[26,27] To our knowledge, experiments using porous 3D scaffolds designed to investigate the zonal organization of tissue-engineered cartilage (e.g., using pore gradients) have not been reported. These studies offer considerable challenges based on the ability to both fabricate and characterize complex, anisotropic scaffold architectures in order to relate concomitant tissue responses to these architectures.

We previously described a novel 3D fiber deposition technique that allows accurate design of polymer scaffolds with controlled porosity, pore size, and mechanical properties for cartilage tissue-engineering applications.[28,29] When compared with traditional foam scaffold architectures with the same porosity, we demonstrated that 3D-deposited scaffold architectures, with 100% interconnecting pores, promoted a more homogeneous distribution of chondrocytes and ECM components as well as enhanced chondrocyte differentiation (i.e., GAG:DNA content) in bovine chondrocytes *in vivo*[29] and human nasal chondrocytes *in vitro*.[30] By further adapting this 3D scaffold technology, the initial aim of this study was to design model 3D fiber-deposited scaffolds containing (1) homogeneously sized pores or pore-size gradients, (2) a similar scaffold volume fraction (i.e., surface-to-volume ratio), (3) similar overall porosity for cell attachment and ECM synthesis, and (4) a 100% interconnecting pore volume to promote cell infiltration and maximize nutrient/waste exchange throughout. Because seeding techniques can also influence the distribution of cells within porous polymeric scaffolds,[31] we adopted two techniques that allowed either a random cell distribution or the direct placement of cells, that is, dynamic seeding in stirred suspension (spinner flask) and static cell injection, respectively. For the static seeding method, scaffolds containing homogeneously sized pores or pore-size gradient were constructed with a dense basal film to prevent cell loss through the highly interconnected pore volume.

Finally, the main aim of the study was to quantitatively evaluate zonal chondrocyte distribution and organization of cartilage ECM components, as measured by DNA, glycosaminoglycan (GAG), and collagen type II content, in response to these model scaffold geometries and seeding regimens after *in vitro* culture. Furthermore, results comparing zonal cell and ECM formation on scaffolds *in vitro* with native bovine articular cartilage are reported herein.

MATERIALS AND METHODS

3D-deposited scaffolds

Porous poly(ethylene glycol)-terephthalate–poly(butylene terephthalate) (PEGT/PBT) copolymer scaffolds (PEG molecular weight, 300; PEGT wt%, 55; PBT wt%, 45) were produced by a novel 3D fiber deposition technique described previously.[28] Briefly, scaffolds were constructed by successively layering a 0–90° pattern of molten copolymer from a 250-μm-diameter nozzle onto a computer-controlled *x–y–z* table. By programming different fiber deposition paths into the computer software, it was possible to generate a range of scaffold architectures by accurately controlling the fiber spacing from one layer to another.[28]

In this study, various scaffold architectures were produced with either a homogeneous 1-mm fiber spacing (*1mm*) or a gradient in fiber spacing (*Grad*) throughout the height of the construct. More specifically, *Grad* scaffolds were constructed by initially depositing four 0–90° layers with a fiber spacing of 2.0 mm, followed by another four layers at 1.0 mm, and finally only one layer at 0.5 mm at the upper surface (Fig. 1B). Therefore, the 2.0 mm-spaced region represented the deep zone, or lower 45% of the scaffold (labeled *L*); the 1.0 mm-spaced region represented the middle zone, or middle 45% of the scaffold (labeled *M*); and the 0.5 mm-spaced region represented the upper zone, or superficial 10% (labeled *S*) of the scaffold (Fig. 1A). In addition, scaffolds with a homogeneous 1-mm fiber spacing (*1mmF*) or a pore gradient (*GradF*) were also produced by directly depositing fibers on a dense PEGT/PBT film (Figs. 1B and 2) approximately 50 μm in thickness in order to provide a barrier to cell and nutrient infiltration, similar to that present within the bone–cartilage interface in articulating joints (Fig. 1A). Films were solution cast from the same PEGT/PBT copolymer composition as the 3D scaffolds, using a technique described previously.[32]

For cell culture experiments, cylindrical samples (7 mm in diameter by 4.0 mm) were cored from bulk 3D-deposited *Grad*, *1mm*, *GradF*, and *1mmF* blocks. Before cell seeding, scaffolds were sterilized by γ irradiation (minimum dose, 25 kGy) in a JS6500 tote box irradiator (Isotron, Ede, The Netherlands).

Scaffold characterization

Because of the regular pore geometry, determining the interconnecting pore size of the resulting scaffolds was possible by scanning electron microscopy (SEM). Theoretical volume percent (vol%) porosity was calculated for each scaffold by using deposition geometries based on a unit cube, whereby the fiber diameter and spacing between layers were equal (i.e., no overlap due to fusion between fibers from one layer to another was assumed), as described previously.[28]

The scaffold volume fraction within each of the *S*, *M*, and *L* zones was also calculated from deposition geometry data. Assuming a unit cube, the fiber surface area (mm^2) equaled *pdln*, where *d*, *l*, and *n* represent the fiber diameter (250 μm), fiber length, and total number of fibers in a given zone, respectively. Values were normalized to the associated volume (mm^3) of each of the *S*, *M*, and *L* zones, by calculating the cross-sectional area (l^2) and height (*h*) of each zone, yielding the zone volume fraction (mm^{-1}) as follows:

$$\text{Zone volume fraction} = \pi dln/l^2h = \pi dn/lh \quad (1)$$

Tissue culture

Bovine chondrocytes were isolated by collagenase digestion (0.15% type II collagenase; Worthington Biochemical, Lakewood, NJ) from articular cartilage harvested from the peripatellar groove of three 6-month-old calf knee joints, and pooled. Full-thickness core samples of articular cartilage (4 mm in diameter by 4.0 mm thick) were also harvested from the same joints to allow comparison of histological and biochemical data with tissue-engineered constructs.

For *Grad* and *1mm* scaffolds, primary cells were dynamically seeded (Fig. 2) on scaffolds (7 mm in diameter by 4.0 mm thick) in spinner flasks (100-mL working volume, 50 rpm; Bellco Glassware, Vineland, NJ) at a density of 8×10^6 cells per scaffold (56 scaffolds in total). For *GradF* and *1mmF* scaffolds, primary cells were statically seeded by placing a highly concentrated cell suspension directly on top of the constructs (8×10^6 cells in a 40-μL cell suspension per scaffold), using a micropipette (Fig. 2). To prevent cell loss through the highly interconnected pores of the 3D scaffolds, *GradF* and *1mmF* constructs were placed within sterile tubing before seeding. Therefore, with the radial borders of the scaffold surrounded by tubing, and a dense film present at the base of the scaffold, only the upper surface remained open. Cells were allowed to settle for 3 h within the scaffolds before being transferred to 12-well plates containing 3 mL of medium. For all samples, the culture medium contained HEPES-buffered Dulbecco's modified Eagle's medium (DMEM; Invitrogen, Carlsbad, CA) supplemented with 10% fetal bovine serum (FBS; Sigma-Aldrich, St. Louis, MO), 0.2 m*M* ascorbic acid 2-phosphate (Invitrogen), 0.1 m*M* nonessential amino acids (Sigma-Aldrich), 0.4 m*M* proline (Sigma-Aldrich), penicillin (100 units/mL; Invitrogen), and streptomycin (100 μg/mL; Invitrogen).

Seeding was evaluated after 3 days of spinner flask (*Grad* and *1mm*) or static (*GradF* and *1mmF*) culture conditions. After removing the tubing on statically seeded scaffolds, all remaining samples were transferred to spinner flasks and remained in culture until day 21, with medium refreshment every 3–4 days. *Grad*, *GradF*, and *1mmF* scaffolds were oriented vertically in spinner flasks so that 0.5 mm-spaced fibers were on top, and the 2 mm-spaced or dense films were at the bottom.

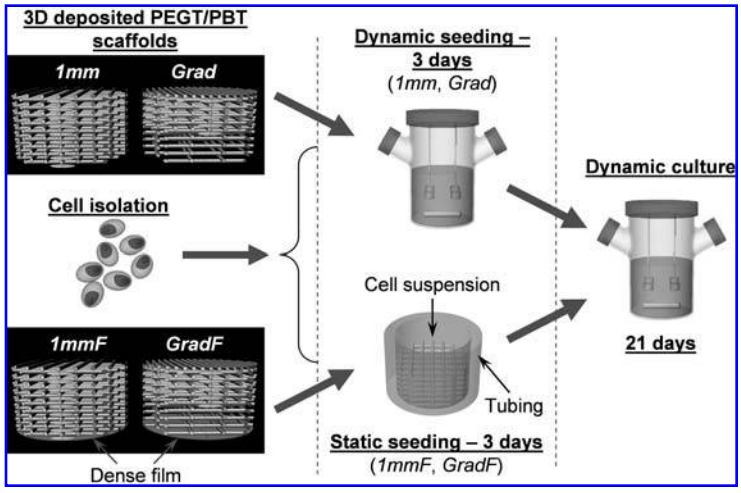

FIG. 2. Overview of 3D-deposited scaffold architectures and *in vitro* seeding and culture techniques. After cell isolation, *1mm* and *Grad* scaffolds were dynamically seeded for 3 days in spinner flasks, whereas *1mmF* and *GradF* scaffolds (containing a dense base film and constrained with sterile tubing) were seeded statically for 3 days. All constructs were transferred to spinner flasks and cultured for 21 days.

Biochemical analysis

Tissue-engineered constructs for biochemical analysis ($n = 3$ per condition at each time point) were sectioned in the three *S*, *M*, and *L* zones indicated in Fig. 1B, using a custom-designed device allowing perpendicular sections of desired thickness to be made with a micrometer. The diameter and thickness of each of the sections were measured with digital calipers (Matsushita, Tokyo, Japan) so that quantitative data from each zone could be normalized by volume as described below. Sections were then placed in a solution containing proteinase K (1 mg/mL), pepstatin A (10 μg/mL), and iodoacetamide (185 μg/mL) (Sigma-Aldrich) overnight at 56°C to digest the cells and extracellular matrix (ECM). These samples were then evaluated for DNA, GAG, and collagen type II content as follows.

DNA content. Quantification of total DNA was performed with a CyQUANT dye kit (Molecular Probes, Eugene, OR) as per the manufacturer's instructions, using a fluorescence plate reader (PerkinElmer, Norwalk, CT).

GAG content. GAG was quantitatively determined by reaction with dimethyl-methylene blue dye (Sigma-Aldrich).[33] Intensity of color change was immediately measured with a microplate reader (EL 312e; Bio-Tek Instruments, Winooski, VT) at an absorbance 520 nm. Values were compared with those from a standard of chondroitin sulfate B (Sigma-Aldrich).

Collagen type II content. By applying an enzyme-linked immunosorbent assay to aliquots of proteinase K digests, collagen type II content was determined as described previously.[34,35]

To allow comparison with native articular cartilage organization, the above-described biochemical assays were performed on corresponding zones (i.e., *S*, *M*, and *L*) of bovine articular cartilage cylinders (4 mm in diameter by 4.0 mm thick), harvested from the same tissue used for cell isolation. Furthermore, to compare the results between the different *S*, *M*, and *L* zones, quantitative biochemical data were normalized by available pore volume (mm^3) within each zone. This was calculated by taking the total volume of the sample ($\pi/4D_c^2t$) based on direct diameter (D_c) and thickness (t) measurements of the construct taken during sectioning, and subtracting the fiber volume. Because the scaffold diameter (D), height (h), and vol% porosity (P) for each zone (excluding tissue) were known from deposition geometries, fiber volume of each zone could be determined according to Eq. (2):

$$\text{Fiber volume} = \text{scaffold volume} \cdot [(100 - \% \text{ porosity})/100] = (\pi/4)D_c^2h \cdot [(100 - P)/100] \quad (2)$$

Histological analysis

Histology. Samples were fixed overnight in 0.14 *M* cacodylate buffer (pH 7.2–7.4) containing 0.25% glutaraldehyde (Merck, Darmstadt, Germany). Samples were then dehydrated in a sequential ethanol series, plastic embedded in glycol methacrylate (Merck), and cut with a microtome to yield 5-μm-thick sections. Sections were stained with hematoxylin (Sigma-Aldrich) and fast green (Merck) to visualize cells/cell nuclei and with safranin O (Sigma-Aldrich) to visualize extracellular glycosaminoglycan (GAG).

Immunohistochemistry. Constructs were embedded in optimal cutting temperature compound (Tissue-Tek O.C.T.; Sakura Finetek USA, Torrance, CA) and snap frozen at −60°C. Cryosections, 5 μm in thickness, were made with a cryotome (Thermo Shandon, Pittsburgh, PA) and fixed in acetone for 8 min. Collagens type I and II were immunolocalized with an Animal Research kit (DakoCytomation, Carpinteria, CA) in combination with collagen type I (Ab-1, diluted 1:1000; Calbiochem, EMD Biosciences, CA) and collagen type II antibodies (II-II6B3, diluted 1:200; Developmental Studies Hybridoma Bank, University of Iowa, Iowa City, IA) as described previously.[36] Staining was visualized with diaminobenzidine (DAB) solution (DakoCytomation) for 5 min in addition to counterstaining with hematoxylin (Sigma-Aldrich).

All histological sections were mounted and examined under a light microscope (Nikon Eclipse E600) with representative images captured with a digital camera (Sony, Tokyo, Japan) and Matrix Vision software (Matrix Vision, Oppenweiler, Germany).

Scanning electron microscopy. Cultured constructs were fixed and dehydrated as described above. To obtain full-thickness cross-sections at right angles to the scaffold fibers, sections were made with a sharp blade scalpel before critical point drying from liquid carbon dioxide (CPD 030 critical point dryer; Bal-Tec, Balzers, Liechtenstein). Samples were then sputter coated (Cressington Scientific, Watford, UK) with a thin gold layer and studied with a Philips XL30 environmental scanning electron microscope (ESEM). Full-thickness cross-sections of as-produced scaffolds were also made with a blade scalpel, before gold sputtering and SEM analysis as described above.

Statistics

To compare biochemical composition between the various zones within each scaffold, one-way analysis of variance (ANOVA) was performed with SigmaStat statistical software (SPSS, Chicago, IL). If tests for normality and variance passed, then one-way ANOVA was per-

formed, whereas if variance tests failed, then one-way ANOVA on ranks was performed with Student–Newman–Keuls post hoc tests for significance ($p < 0.05$) used in both cases.

RESULTS

Scaffold characterization

As shown in Fig. 3, the desired overall volume percent porosity (80.1 and 78.0%) and volume fraction (3.25 and 3.69 mm^{-1}) available for cell attachment and ECM formation were similar for both *Grad* and *1mm* scaffolds, respectively. As expected, the *S* zone, with 0.5-mm fiber spacing in *Grad* and *GradF* scaffolds, had the lowest porosity and highest volume fraction (59.2% and 6.67 mm^{-1}, respectively), whereas the *L* zone, with 2.0-mm fiber spacing, had the highest porosity and lowest volume fraction (87.4% and 2.05 mm^{-1}, respectively). The *M* zone, with 1.0-mm fiber spacing, had a porosity and volume fraction of 78.0% and 3.59 mm^{-1}, respectively. The porosity and volume fraction values of the latter were also characteristic of each of the *S*, *M*, and *L* zones in *1mm* and *1mmF* scaffolds, as they contained the same homogeneous 1.0-mm fiber spacing throughout (Fig. 3).

The average interconnecting pore size present within scaffold zones produced with 0.5-, 1.0-, or 2.0-mm fiber spacing was 192 ± 47, 677 ± 39, and 1650 ± 75 μm, respectively, and was consistent with previous SEM analysis of 3D-deposited scaffold architectures.[28] Furthermore, parallel studies have demonstrated excellent agreement between predicted values for porosity and volume fraction of 3D-deposited scaffold architectures compared with microcomputed tomography analysis.[29,30] Therefore, considerably different and distinct variations in pore size, porosity, and volume fraction were available within *Grad* scaffold zones for observing cellular responses.

Biochemical analysis

DNA. DNA results showed a significantly higher concentration of cells per unit volume in *Grad* and *GradF S* zones than in corresponding *M* and *L* zones, respectively, on both day 3 and day 21 (Fig. 4A). This anisotropic cell distribution, particularly on day 3, was similar to that measured in bovine articular cartilage explants, where we observed a significantly higher concentration of cells per unit volume within the *S* zone compared with *M* and *L* zones (Fig. 4B). In comparison, *1mm* and *1mmF* scaffolds, without a pore volume gradient, showed a more homogeneous distribution of cells per unit volume across the three *S*, *M*, and *L* zones. In these scaffolds, a significant difference in cell number was observed only be-

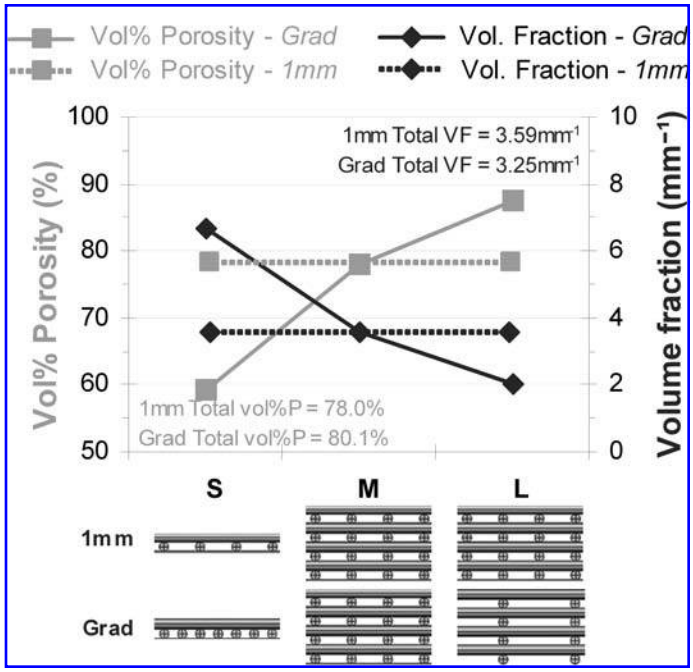

FIG. 3. Zonal distribution in porosity (shaded symbols) and volume fraction (solid symbols) measured for *S*, *M*, and *L* zones within *Grad* (solid lines) and *1mm* (dotted lines) scaffolds. While volume percent (vol%) porosity and volume fraction (VF) within each zone in *Grad* scaffolds varied between 59–84% and 2.05–6.67 mm^{-1}, respectively, the total vol% porosity and volume fraction available for cell infiltration and attachment throughout all zones within both *Grad* and *1mm* scaffolds were similar (80.1 versus 78.0% and 3.25 versus 3.69 mm^{-1}, respectively).

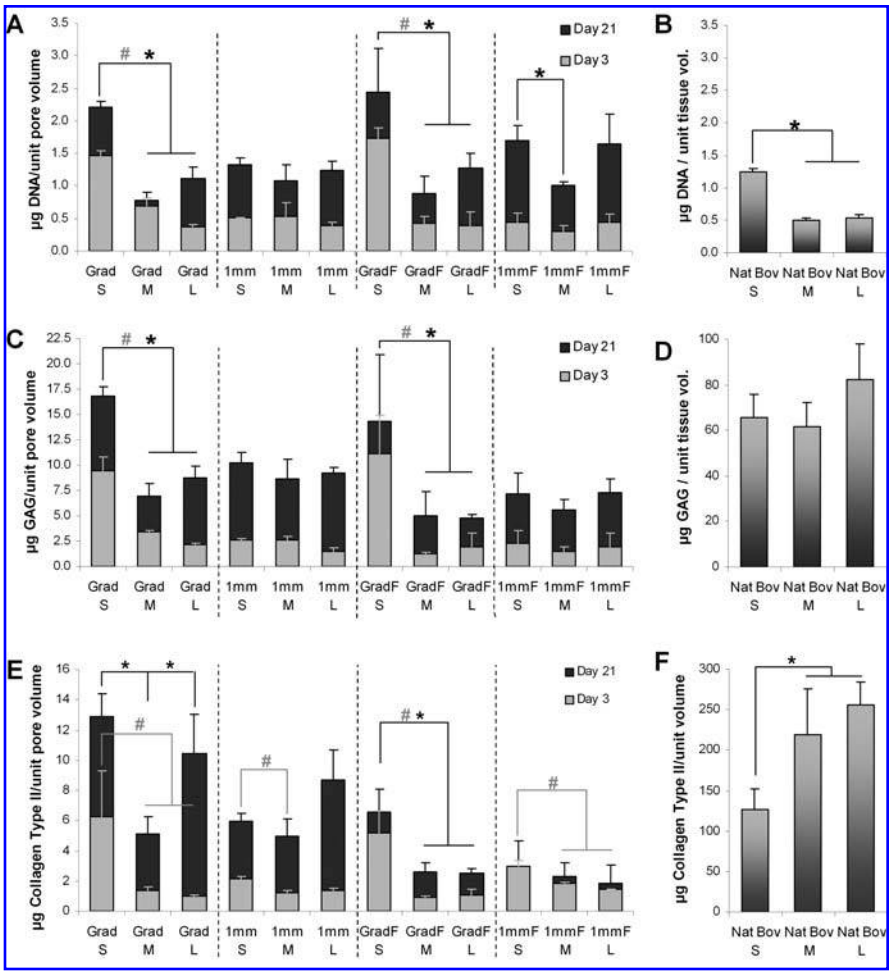

FIG. 4. Zonal distribution in (**A** and **B**) cell number (DNA content), (**C** and **D**) GAG content, and (**E** and **F**) collagen type II content within *Grad*, *1mm*, *GradF*, and *1mmF* constructs after seeding on day 3 (shaded portion of columns) and at 21 days of tissue culture (solid portion of columns) compared with native bovine articular cartilage explants (**B**, **D**, and **F**). For each scaffold architecture, constructs were sectioned into their corresponding *S* (10%), *M* (45%), and *L* (45%) zones and analyzed separately. A significant difference between *S*, *M*, and *L* zones is denoted as follows: #day 3; *day 21.

tween *1mmF S* and *M* zones on day 21 and was likely the result of the static seeding technique, which resulted in the cells settling either within the upper fibers or deep near the dense film (Fig. 6C).

When comparing the DNA per unit volume with the volume fraction for *Grad and GradF* scaffolds (Fig. 5A and C), we saw a direct correlation between cellularity and scaffold volume fraction on day 3 in gradient scaffolds ($R^2 = 0.997$ and 0.908, respectively), but to a lesser extent after 21 days of culture ($R^2 = 0.715$ and 0.706, respectively).

GAG. GAG results showed an anisotropic distribution similar to that of the DNA data. Again, *Grad* and *GradF S* zones contained a significantly higher GAG content than *M* and *L* zones, respectively, both on day 3 and day 21 (Fig. 4C). These significant trends were not seen in *1mm* and *1mmF* scaffolds. GAG per unit volume in native bovine articular cartilage explants was highest in the *L* zone; however, this was not significantly higher than in *S* and *M* zones (Fig. 4D). Furthermore, the amount of GAG measured in native cartilage was approximately 5 to 10 times higher than in the corresponding zones within cultured scaffolds.

As shown in Fig. 5B and D, there was also a direct correlation between GAG content and volume fraction for *Grad* scaffolds on day 3 ($R^2 = 0.970$), but to a lesser extent for *GradF* scaffolds ($R^2 = 0.855$). Conversely, on day 21, GAG content more directly correlated with volume fraction in *GradF* scaffolds ($R^2 = 0.904$) compared with *Grad* scaffolds ($R^2 = 0.762$).

GAG:DNA. When GAG content was normalized to DNA for each zone in native cartilage explants, significantly higher GAG:DNA was present in the *L* zone compared with *M* and *S* zones, respectively (Fig. 1). There

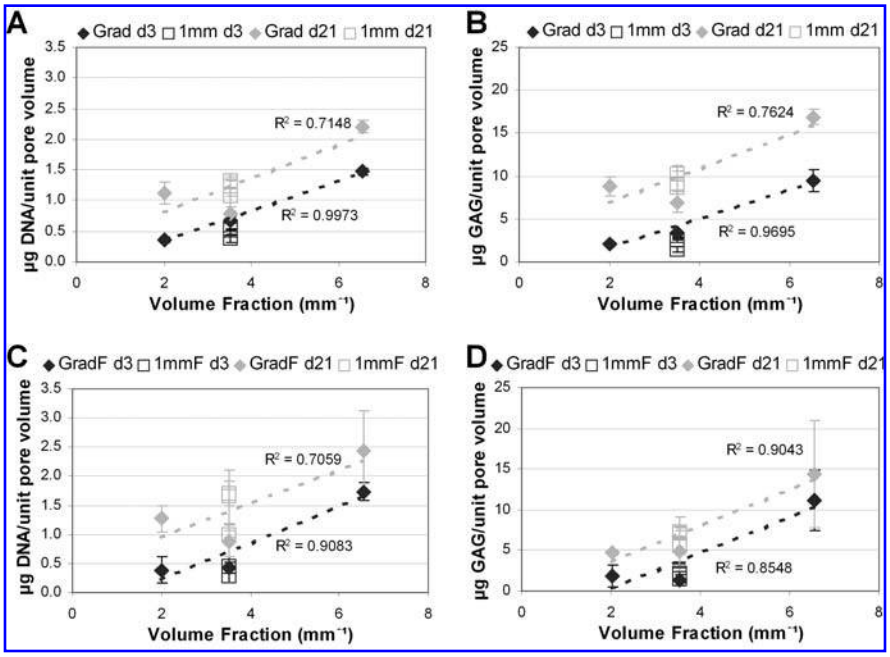

FIG. 5. Least-squares fit showing the correlation between cell number (DNA content) (**A** and **C**) and GAG content (**B** and **D**) with scaffold volume fraction (i.e., surface-to-volume ratio) in *Grad*/*1mm* scaffolds (**A** and **B**) and *GradF*/*1mmF* scaffolds (**C** and **D**) after 3 days of seeding and after 21 days of tissue culture. Because volume fraction remains constant for *1mm* and *1mmF* scaffolds, R^2 values are illustrated for *Grad* and *GradF* scaffolds at each time point.

was no significant difference in GAG:DNA within respective zones of cultured scaffolds with and without pore volume gradients (data not shown). However, GAG:DNA content in *Grad* and *1mm* scaffolds increased between day 3 and day 21, whereas, for *GradF* and *1mmF* scaffolds, GAG:DNA remained unchanged with culture time (data not shown).

Collagen type II. An anisotropic distribution in collagen type II content per unit volume was also observed in *Grad* and *GradF* scaffolds on day 3 and day 21, although some significant differences were seen in *1mm* and *1mmF* scaffolds on day 3 (Fig. 4E). In general, *S* zones of *Grad* and *GradF* contained significantly higher collagen type II compared with *M* and *L* zones. The exception was between *Grad S* and *L* zones, which exhibited the highest levels of collagen type II, but were not significantly different from one another. Notably, however, a 10-fold increase in collagen II content was observed between day 3 and day 21 in zone *L*, whereas only a 2-fold increase was observed in the *S* zone (Fig. 4E). Therefore, on the basis of the rate of collagen synthesis, longer culture periods might result in a distribution of collagen type II more similar to native articular cartilage explants illustrated in Fig. 4F. In this case, we observed significantly greater amounts of collagen type II per unit volume in *L* and *M* zones than in the *S* zone (Fig. 4F). Similar to GAG data, collagen type II content per unit volume within native cartilage was approximately 10 times higher than values measured in cultured samples and, compared with *Grad* and *1mm* scaffolds, increases in collagen content between day 3 and day 21 for *GradF* and *1mmF* scaffolds remained limited. Possible reasons for these observations in *GradF* and *1mmF* scaffolds may have again been related to cell damage during the static seeding process. Alternatively, the greater concentration of cells located within the center of *1mmF* scaffolds after static seeding (Fig. 6C) may have limited cell nutrient and waste exchange in these scaffolds. As a result, cells perhaps were more likely to proliferate with compromised GAG and collagen synthesis. *GradF* scaffolds also performed poorly and the greater number of cells in the S zone and possible better access to initial nutrient supply and fluid flow though large pores in the *L* zone may be responsible for marginally greater collagen II synthesis compared with *1mmF* scaffolds.

Histological analysis

SEM and GAG. SEM and safranin O-stained sections showed that after 3 days of dynamic seeding in spinner flasks, single cells, but more predominantly cell aggregates, were homogeneously distributed throughout *1mm* (Fig. 6A) and *Grad* (Fig. 6B) scaffolds, essentially covering all available fiber surface area (Fig. 6A and B, insets). Because of the higher density of

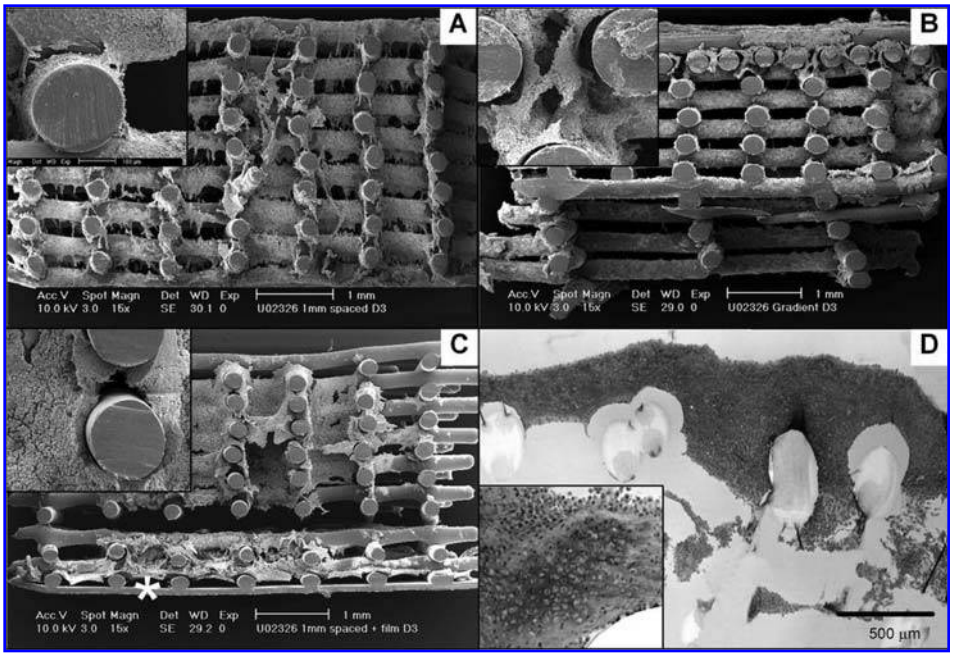

FIG. 6. SEM (**A**–**C**, ×15) and safranin O-stained sections (**D**) showing cell attachment and morphology on *1mm* (**A**), *Grad* (**B** and **D**), and *1mmF* (**C**) scaffolds after 3 days of seeding. Available fiber surfaces of spinner flask-seeded *1mm* and *Grad* scaffolds were nearly completely covered with a layer of cells/cell aggregates (**A** and **B** [insets], ×150). Statically seeded scaffolds [*1mmF* shown in (**C**)] contained localized regions of high cell density (**C** [inset], ×150), often bridging between fibers at the center and base of the scaffold, resulting in cell-free regions at the periphery (*50-μm-thick dense film).

fibers in the upper *S* zone of *Grad* scaffolds, there appeared to be a greater concentration of cells in this zone compared with *M* and *L* zones, respectively (Fig. 6B), as previously confirmed in DNA assays (Fig. 4A), with cell aggregates bridging between 0.5 mm-spaced fibers (Fig. 6B, inset). In contrast to the more random seeding of cells in spinner flasks, static seeding of a highly concentrated cell suspension on *GradF* (not shown) and *1mmF* (Fig. 6C) scaffolds resulted in a less homogeneous cell distribution, leaving cell-free regions at the periphery of the scaffolds. This was likely due to the homogeneous 1-mm fiber spacing, which allowed cells to progress more easily through the interconnecting pore volume with static seeding. Central pores in these statically seeded scaffolds tended to have considerable bridging of cell aggregates (Fig. 6C, inset). Importantly, the dense basal film prevented these cells from exiting the scaffold. Positive safranin O staining for GAG was evident in the tissue surrounding fibers in all scaffolds after 3 days (e.g., *Grad* shown in Fig. 6D). The intensity of GAG staining within scaffolds tended to be greatest in regions of highest cell concentration and, therefore, *S* zones in *Grad* and *GradF* scaffolds exhibited more regions of positive GAG staining (Fig. 6D), thus confirming our biochemical GAG findings (Fig. 4C). In all cases, attached cells had aggregated around the PEGT/PBT fibers in multiple cell layers and had a rounded morphology (Fig. 6D, inset).

After 21 days of culture, SEM and safranin O-stained sections showed tissue formation within interconnecting pores of all scaffolds with ECM bridging the gaps between fibers and resulting in consistent GAG staining (e.g., *1mm* and *Grad*; Fig. 7A and B). The exception was ECM formation within *L* zones in *Grad* (Fig. 7B) and *GradF* (Fig. 7D) scaffolds, where there was incomplete bridging between fibers and areas of void space still remaining unfilled. Qualitatively, the amount of cells and GAG staining present within the various *S*, *M*, and *L* zones was consistent with biochemical DNA and GAG data, particularly with the higher content of DNA and GAG within the upper *S* zone of *Grad* and *GradF* scaffolds. In contrast, the homogeneous pore distribution in *1mm* (Fig. 7A) and *1mmF* scaffolds (Fig. 7C) tended to result in a more homogeneous cell and GAG distribution (Fig. 7E). In all scaffolds, a thin fibrous capsule, approximately 100 μm thick, was present at the periphery of all scaffolds cultured for 21 days (e.g., *1mm* and *Grad*; Fig. 7E and F), and was likely related to the dynamic fluid flow imparted on the cells at the periphery of the scaffold during spinner flask culture.[37] ECM within this thin layer did not stain positively for GAG and contained flattened, more fibroblast-like cells similar to the super-

ficial zone of native bovine cartilage (see safranin O staining in Fig. 1).

Immunohistochemistry. Collagen type I and II immunostaining was performed on scaffolds cultured for 21 days only, as we expected limited collagen synthesis to have occurred at the 3-day time point. Within *Grad*, *1mm*, *GradF*, and *1mmF* scaffolds, collagen type II was clearly expressed in each zone (e.g., *1mm* and *Grad*; Fig. 7G and I). Collagen type I was expressed only at the periphery of the scaffolds in correlation with the fibrous capsule (e.g., *1mm* and *Grad*; Fig. 7H and J). Interestingly, because of the film in *GradF* and *1mmF* scaffolds, no fibrous capsule formed in *L* zones, resulting in only collagen type II expression and not type I (not shown). With respect to collagen orientation in scaffolds, we were unable to clearly comment on a recapitulation of the radial collagen orientation present in native cartilage (see collagen II in Fig. 1) after 21 days.

DISCUSSION AND CONCLUSIONS

The aim of this study was not to completely recapitulate the zonal cell and ECM distribution of articular cartilage, but to describe a preliminary model to investigate whether scaffolds designed with pore volume gradients could be instructive for cell and/or ECM distribution. Using a novel computer-controlled 3D fiber deposition technique,[28] we successfully produced scaffolds with 100% interconnecting porous architectures with pores that were either homogeneous (*1mm*) or gradated in size (*Grad*) (Fig. 1A). This accurate control over scaffold design allowed direct comparisons to be made, relating cell and tissue responses to scaffold pore architectures. For comparison with tissue-engineered constructs, we also described a technique to determine the zonal distribution of DNA, GAG, and collagen type II within *S*, *M*, and *L* zones in 4.0-mm-thick native bovine articular cartilage explants. This technique was verified by quantitative biochemical data and qualitative histology and immunohistochemistry techniques, and were consistent with previous studies demonstrating the organizational structure of native articular cartilage.[5,10] Cell attachment to PEGT/PBT fibers was achieved by two seeding techniques. Dynamic spinner flask seeding was used to randomly introduce cells to various scaffolds, whereas static cell seeding was used to offer a level of control over cell placement within various scaffolds. Statically seeded scaffolds (*GradF* and *1mmF*) contained a dense film to confine cells within the porous architectures. By using a static seeding method, we hoped to further control the placement of cells, based on the expectation that most of the cell suspension would remain in the upper *S* zone of *GradF* and *1mmF* scaffolds, with some cells gravitating toward the basal dense film through the large interconnecting pores.

Few studies have systematically investigated the effect of pore size on chondrocyte behavior; however, it has been suggested that in scaffolds containing small pore sizes (<20 μm), cell–cell interactions are enhanced, resulting in improved chondrocyte proliferation and GAG content,[38] whereas total collagen content[39] and collagen type II[40] are little affected by pore size and geometry. Scaffolds used in these studies were suboptimal, however, for comparison of effects between biodegradable substrates of different composition that also changed shape with time in culture,[38] or did not support tissue formation throughout, but rather on top of scaffolds.[39] Moreover, investigators have not typically evaluated scaffolds with 100% interconnecting pores with large variation in size (i.e., typically 20–300 μm in diameter, compared with 200–1650 μm used in this study), or investigated how collagen type II is distributed throughout porous scaffolds. Other reports suggest that pellet or mass cultures, which allow close cell–cell interactions, enhance chondrocyte (re)differentiation (i.e., GAG:DNA content) and ECM matrix production.[41,42] We hypothesized that differences in biochemical content may exist between zones where cell–cell interactions varied greatly, that is, *S* zones (0.5-mm fiber spacing) compared with *L* zones (2.0-mm spacing). Purely on the basis of available zonal pore volume and on the fact that chondrocytes in native cartilage occupy a small percentage of the overall tissue volume ($<2\%$), we had hypothesized that there were physical volumetric limits to the amount of GAG and collagen type II synthesis per cell in *S* zones as opposed to *L* zones, if cells were provided with suitable nutrients and a 3D environment. For example, chondrocytes in *S* zones with high cell–cell interaction would be stimulated to proliferate and rapidly synthesize ECM until the available pore volume was filled, whereupon further ECM formation might reach an equilibrium. On the other hand, chondrocytes in *L* zones, with low cell density, fewer cell–cell interactions, and fewer volumetric limitations could proliferate and, on a per-cell basis, synthesize more GAG and collagen type II, more akin the levels synthesized by cells in the deep zone of native articular cartilage.

By incorporating pore size gradients based on *S*, *M*, and *L* zones, we were able to demonstrate an anisotropic cell and ECM distribution, whereby direct correlations between cell number (DNA content) and GAG content with scaffold volume fraction were observed in *Grad* and *GradF* scaffolds after 3 days of seeding, which was maintained in spinner flask culture up to 21 days. Moreover, this zonal distribution in DNA content within *Grad* and *GradF* scaffolds was shown to be similar to that measured in native bovine articular cartilage. The slightly lower GAG content observed in *GradF* and *1mmF* scaffolds could be related to the dense film blocking fluid

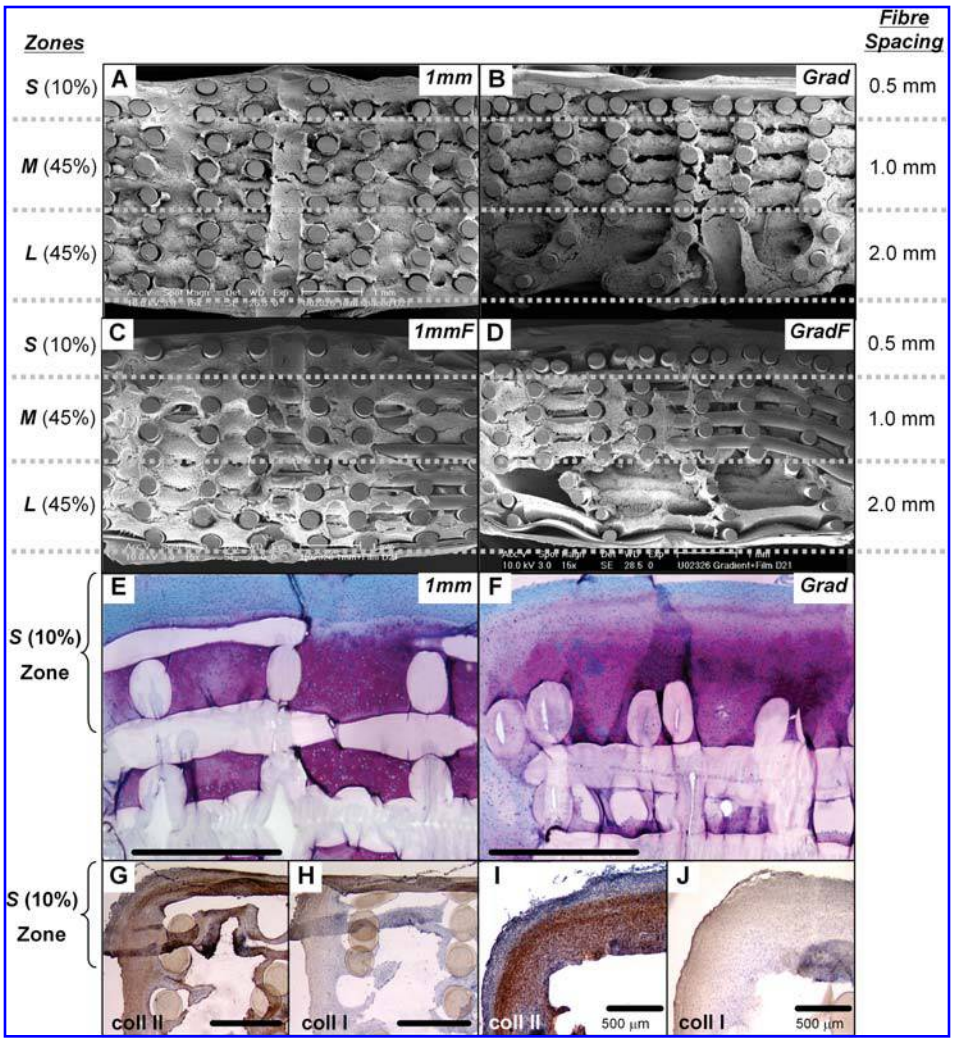

FIG. 7. Representative SEM (**A**–**D**, ×15) and safranin O (**E** and **F**), collagen type II (**G** and **I**), and collagen type I (**H** and **J**) immunohistology sections showing extracellular matrix (ECM) formation within *1mm* (**A**, **E**, **G**, and **H**), *1mmF* (**C**), *Grad* (**B**, **F**, **I**, and **J**), and *GradF* (**D**) scaffolds after 21 days of dynamic culture. Regions corresponding to *S*, *M*, and *L* zones are indicated on the *left*, with associated fiber spacing of *Grad*/*GradF* scaffolds indicated on the *right* (scale bars = 1 mm unless otherwise stated).

flow and/or nutrition to the cells, or the injection seeding technique may have caused greater damage to cells than dynamic seeding (although cell viability was not determined in this case). Pore volume gradients, within the ranges used in this experiment, were not sufficient to elicit noticeable differences in GAG:DNA, particularly in relation to the zonal variations seen in native cartilage.

Similar to DNA and GAG results, anisotropic distributions of collagen type II content per unit volume were observed in *Grad* and *GradF* scaffolds (Fig. 4). Interestingly, after 21 days of culture the collagen type II content in the *Grad L* zone was not significantly different from that in the *S* zone, with a 10-fold increase in accumulation from day 3 (Fig. 4E). Because DNA content in the *L* zone was significantly lower than in the *S* zone on day 21 (Fig. 4A), this suggests that in the *L* zone, with its low volume fraction and high porosity, a greater amount of collagen type II was being synthesized per cell than in other zones. This observation was not made, however, in the *L* zone of *GradF* scaffolds, where significantly higher collagen type II content existed in the *S* zone compared with both *M* and *L* zones. It is intuitive to expect zones of high cell density per unit volume (i.e., the *S* zone) to synthesize greater amounts of collagen; however, there may be another mechanism operating in the *L* zone of *Grad* scaffolds related to the low cell number, low volume fraction, and large pore size. SEM and safranin O-stained sections demonstrated that few of the large pores within *Grad* scaffolds were completely filled with ECM after 21 days (Fig. 7E). Therefore, with fewer

cell–cell interactions and incomplete bridging of about 1650 μm-sized pores compared with *S* and *M* zones, it was likely that more cells were exposed to dynamic fluid flow conditions resulting in stimulation of higher collagen type II synthesis per cell.[43] This is further evidenced in *GradF* scaffolds where, even though few of the large pores were filled with ECM after 21 days, fluid flow was likely inhibited in the *L* zone by the dense film, resulting in reduced collagen type II synthesis compared with the *L* zone of *Grad* scaffolds. These results also raise the possibility that pore geometry affects the synthesis of GAG and collagen II differently, even by cells within the same scaffold. Perhaps longer culture periods would allow ECM to completely fill these *L* zones, resulting in significant variations in zonal collagen type II content more in line with that present in native articular cartilage (Fig. 6B). Although we did observe zonal variations in collagen type II synthesis per cell, based on available pore volume in this study, we could not confirm this hypothesis, and further studies are required to understand possible mechanisms and/or alternative methods are needed to control zonal cell behavior.

Other studies have attempted to address the need for developing scaffolds or culture techniques that (re)create repair tissue resembling the zonal organization within articular cartilage. In general, these studies have adopted the use of polymer, alginate, or agarose gels to spatially distribute chondrocytes isolated from superficial, middle, and deep zone cartilage.[10,23,24,27] Although these studies have promising advantages in that the desired cells and cell concentrations can be easily incorporated in a 3D environment, and that specific zonal markers, such as superficial zone protein, or differential accumulation of GAG and total collagen can be achieved, they do offer some limitations. First, it is difficult to isolate chondrocytes from separate zones in articular cartilage, particularly for human tissue where the zonal differences are less distinct and biopsies are limited in size. Second, these gels typically have limited mechanical properties compared with native cartilage and the gels also contain distinct boundaries between zones that could delaminate as a result of shear stresses.

We describe in this study an alternative method for studying zonal organization within tissue-engineered cartilage constructs. By controlling the design of scaffolds by 3D fiber deposition, we were able to influence the number and distribution of cells and, to a certain extent, their ability to produce zonal ECM components by varying the volume fraction and pore volume distribution within a single scaffold. The computer-controlled nature of the 3D fiber deposition process also allows accurate and reproducible bonding of PEGT/PBT fibers, integrating one zone into another, irrespective of architecture, so that complex gradient scaffolds can be produced with a thickness similar to that of articular cartilage (2–6 mm). Furthermore, we have previously demonstrated how fiber spacing and deposition patterns can be tailored to produce scaffolds with dynamic mechanical properties similar to those of articular cartilage.[28] For example, 3D-deposited PEGT/PBT scaffolds with 1.0-mm fiber spacing exhibited a compressive dynamic stiffness (at 0.1 Hz) of 4.3 ± 0.5 MPa compared with the 4.1 ± 1.6 MPa exhibited by bovine articular cartilage, whereas scaffolds with 2.0-mm fiber spacing were significantly less stiff (0.2 ± 0.1 MPa). Although gel techniques offer limited mechanical properties, particularly at the interface from one zone to another, some studies are emerging in which different concentrations of agarose gels have been combined to produce zonal constructs with varying stiffness[24]; however, these are far from matching articular cartilage.

For clinical applications, the ability to incorporate a dense basal layer into the construct, which prevents infiltration of blood- and/or marrow-derived progenitor cells into the wound site, a repair consequence that typically results in inferior fibrocartilage *in vivo* as opposed to the desired hyaline cartilage, may be an important feature in future scaffold designs.[44] We demonstrated that the dense film in *GradF* and *1mmF* scaffolds assisted cell retention with static seeding techniques and could be incorporated into future *in vivo* studies in which both zonal pore gradients and solid barriers to host cell infiltration can be evaluated. It is worth noting that the natural barrier, the layer of calcified cartilage that anchors cartilage to subchondral bone, was not addressed in this zonal study. This limitation should be addressed in future as the calcified cartilage layer forms a critical link with the remaining zonal organization for successful biomechanical function of the articulating joints.[45,46]

One other limitation of the technique presented in this study is that a heterogeneous chondrocyte population (i.e., cells from superficial, middle, and deep zones) was introduced into the scaffold, offering little control over the placement of cells in specific zones, as achieved by previously mentioned gel encapsulation techniques. Previous studies within our group have demonstrated that different compositions of PEGT/PBT copolymers can influence the attachment and phenotypic expression of human articular chondrocytes on both 2D films[47] and on 3D-deposited fiber scaffolds.[30] In future, the flexibility of the 3D fiber deposition technique may allow us not only to control the gradient in pore volume, volume fraction, and mechanical properties, but also to incorporate gradients in PEGT/PBT composition within scaffolds to regulate chondrocyte phenotype, irrespective of cell heterogeneity or zonal origin of the cell. For instance, a high density of fibers from a PEGT/PBT composition, which promotes cell attachment, proliferation, and a more dedifferentiated phenotype (i.e., lower GAG:DNA and collagen II content indicative of more superficial chondrocytes), could be applied at the superficial zone. This

architecture may also provide sufficient mechanical properties to withstand tensile forces at the articulating surface. Whereas, at the deep zone, a lower density of fibers with a PEGT/PBT composition, which promotes a more differentiated phenotype (i.e., higher GAG:DNA and collagen II content), could result in a zonal tissue organization and biomechanical properties more similar to native articular cartilage. The flexibility in PEGT/PBT copolymer composition may also allow us in future to influence the zonal scaffold biodegradation rate,[48] another feature that has been shown to influence deposition of ECM components *in vitro* in hydrogels.[49] In future studies, we intend to address whether such scaffolds will result in enhanced instructive characteristics relative to those presented in this study.

In conclusion, this study provides insight into ways in which instructive characteristics could be incorporated into 3D scaffold designs for tissue engineering articular cartilage that resembles native zonal cell, structural, and mechanical organization. We demonstrated an experimental model for developing porous, 100% interconnected scaffolds with similar pore volume, but containing either homogeneous pores or pore-size gradients. *In vitro* cell seeding showed that pore-size gradients promoted an inhomogeneous cell distribution mimicking that of immature bovine cartilage, irrespective of dynamic or static seeding methods. Prolonged *in vitro* tissue culture showed similar inhomogeneous distributions in zonal GAG and collagen type II. However, gradients in cell–cell interactions based on controlled changes in pore size within *Grad* and *GradF* scaffolds did not influence the zonal distribution of GAG:DNA. Further research employing the techniques used in this study is required in order to recreate the same distributions of GAG and collagen II *in vitro* and *in vivo* as in native articular cartilage.

ACKNOWLEDGMENTS

The authors acknowledge funding from the European Commission ("Scafcart" project G5RD-CT-1999-00050).

REFERENCES

1. Hunziker, E.B. Articular cartilage repair: Are the intrinsic biological constraints undermining this process insuperable? Osteoarthritis Cartilage **7,** 15, 1999.
2. Shapiro, F., Koide, S., and Glimcher, M. Cell origin and differentiation in the repair of full-thickness defects of articular cartilage. J Bone Joint Surg. Am. **75,** 532, 1993.
3. Woodfield, T.B.F., Bezemer, J.M., Pieper, J.S., van Blitterswijk, C.A., and Riesle, J. Scaffolds for tissue engineering of cartilage. Crit. Rev. Eukaryot. Gene Expr. **12,** 209, 2002.
4. Hunziker, E.B. Articular cartilage repair: Basic science and clinical progress. A review of the current status and prospects. Osteoarthritis Cartilage **10,** 432, 2002.
5. Hunziker, E.B., Quinn, T.M., and Hauselmann, H.J. Quantitative structural organization of normal adult human articular cartilage. Osteoarthritis Cartilage **10,** 564, 2002.
6. Mankin, H.J., Mow, V.C., Buckwalter, J.A., Iannotti, J.P., and Ratcliffe, A. Articular cartilage structure, composition and function. In: Buckwalter, J.A., Einhorn, T.A., and Simon, S.R., eds. Orthopaedic Basic Science: Biology and Biomechanics of the Musculoskeletal System. Rosemont, IL: American Academy of Orthopaedic Surgeons, 2000, pp. 443.
7. Buckwalter, J., and Mankin, H. Instructional Course Lectures: American Academy of Orthopaedic Surgeons—Articular Cartilage. I. Tissue design and chondrocyte–matrix interactions. J. Bone Joint Surg. Am. **79,** 600, 1997.
8. Ratcliffe, A., Fryer, P.R., and Hardingham, T.E. The distribution of aggregating proteoglycans in articular cartilage: Comparison of quantitative immunoelectron microscopy with radioimmunoassay and biochemical analysis. J. Histochem. Cytochem. **32,** 193, 1984.
9. Wong, M., Wuethrich, P., Eggli, P., and Hunziker, E. Zone-specific cell biosynthetic activity in mature bovine articular cartilage: A new method using confocal microscopic stereology and quantitative autoradiography. J. Orthop. Res. **14,** 424, 1996.
10. Kim, T.K., Sharma, B., Williams, C.G., Ruffner, M.A., Malik, A., McFarland, E.G., and Elisseeff, J.H. Experimental model for cartilage tissue engineering to regenerate the zonal organization of articular cartilage. Osteoarthritis Cartilage **11,** 653, 2003.
11. Waldman, S., Grynpas, M., Pilliar, R., and Kandel, R. The use of specific chondrocyte populations to modulate the properties of tissue-engineered cartilage. J. Orthop. Res. **21,** 132, 2003.
12. Mow, V.C., and Wang, C.C. Some bioengineering considerations for tissue engineering of articular cartilage. Clin. Orthop. **367,** S204, 1999.
13. Guilak, F., Butler, D.L., and Goldstein, S.A. Functional tissue engineering: The role of biomechanics in articular cartilage repair. Clin. Orthop. **391,** S295, 2001.
14. Chen, A., Bae, W., Schinagl, R., and Sah, R. Depth- and strain-dependent mechanical and electromechanical properties of full-thickness bovine articular cartilage in confined compression. J. Biomech. **34,** 1, 2001.
15. Li, L., Shirazi-Adl, A., and Buschmann, M. Alterations in mechanical behaviour of articular cartilage due to changes in depth varying material properties: a nonhomogeneous poroelastic model study. Comput. Methods Biomech. Biomed. Eng. **5,** 45, 2002.
16. Mow, V.C., and Guo, X.E. Mechano-electrochemical properties of articular cartilage: Their inhomogeneities and anisotropies. Annu. Rev. Biomed. Eng. **4,** 175, 2002.
17. Treppo, S., Koepp, H., Quan, E.C., Cole, A.A., Kuettner, K.E., and Grodzinsky, A.J. Comparison of biomechanical and biochemical properties of cartilage from human knee and ankle pairs. J. Orthop. Res. **18,** 739, 2000.
18. Hubbell, J.A. Bioactive biomaterials. Curr. Opin. Biotechnol. **10,** 123, 1999.

19. Hubbell, J.A. Biomaterials in tissue engineering. Biotechnology **13,** 565, 1995.
20. Hutmacher, D.W. Scaffolds in tissue engineering bone and cartilage. Biomaterials **21,** 2529, 2000.
21. Lin, A.S., Barrows, T.H., Cartmella, S.H., and Guldberg, R.E. Microarchitectural and mechanical characterization of oriented porous polymer scaffolds. Biomaterials **24,** 481, 2003.
22. Slivka, M.A., Leatherbury, N.C., Kieswetter, K., and Niederauer, G.G. Porous, resorbable, fiber-reinforced scaffolds tailored for articular cartilage repair. Tissue Eng. **7,** 767, 2001.
23. Sharma, B., Williams, C.G., Kim, T.K., Malik, A., and Elisseeff, J.H. Multi-layered hydrogel constructs recreate zonal organization of articular cartilage. In: Transactions of the Orthopedic Research Society, 49th Annual Meeting, New Orleans, LA, 2003. Vol. 28, abstract 948.
24. Ng, K., Wang, C.C., Guo, X.E., Ateshian, G.A., and Hung, C.T. Characterization of inhomogeneous bi-layered chondrocyte-seeded agarose constructs of differing agarose concentrations. In: Transactions of the Orthopedic Research Society, 49th Annual Meeting, New Orleans, LA, 2003. Vol. 28, abstract 960.
25. Aydelotte, M., Thonar, E., Mollenhauer, J., and Flechtenmacher, J. Culture of chondrocytes in alginate gel: Variations in conditions of gelation influence the structure of the alginate gel, and the arrangement and morphology of proliferating chondrocytes. In Vitro Cell. Dev. Biol. Anim. **34,** 123, 1998.
26. Thomson, B., Smith, M., Boyer, S., Turner, R., Kidd, D., Riggs, H., Dowthwaite, G., and Archer, C. Coated biomaterials, zonal cell-seeding and cartilage tissue engineering. In: Transactions of the Orthopedic Research Society, 48th Annual Meeting, Dallas, TX, 2002. Vol. 27, abstract 477.
27. Klein, T.J., Schumacher, B.L., Li, K.W., Voegtline, M., Masuda, K., Thonar, E.J., and Sah, R.L. Tissue engineered articular cartilage with functional stratification: Targeted delivery of chondrocytes expressing superficial zone protein. In: Transactions of the Orthopedic Research Society, 48th Annual Meeting, Dallas, TX, 2002. Vol. 27, abstract 212.
28. Woodfield, T.B.F., Malda, J., de Wijn, J., PÇters, F., Riesle, J., and van Blitterswijk, C.A. Design of porous scaffolds for cartilage tissue engineering using a three-dimensional fiber-deposition technique. Biomaterials **25,** 4149, 2004.
29. Malda, J., Woodfield, T.B.F., van der Vloodt, F., Wilson, C., Martens, D.E., Tramper, J., van Blitterswijk, C.A., and Riesle, J. The effect of PEGT/PBT scaffold architecture on the composition of tissue engineered cartilage. Biomaterials **26,** 2005.
30. Miot, S., Woodfield, T.B.F., Daniels, A.U., Suetterlin, R., Peterschmitt, I., Heberer, M., van Blitterswijk, C.A., Riesle, J., and Martin, I. Effects of scaffold composition and architecture on human nasal chondrocyte redifferentiation and cartilaginous matrix deposition. Biomaterials **26,** 2005.
31. Vunjak-Novakovic, G., Obradovic, B., Martin, I., Bursac, P., Langer, R., and Freed, L. Dynamic cell seeding of polymer scaffolds for cartilage tissue engineering. Biotechnol. Prog. **14,** 193, 1998.
32. Papadaki, M., Mahmood, T., Gupta, P., Claase, M.B., Grijpma, D.W., Riesle, J., van Blitterswijk, C.A., and Langer, R. The different behaviors of skeletal muscle cells and chondrocytes on PEGT/PBT block copolymers are related to the surface properties of the substrate. J. Biomed. Mater. Res. **54,** 47, 2001.
33. Farndale, R., Buttle, D., and Barrett, A. Improved quantitation and discrimination of sulphated glycosaminoglycans by use of dimethylmethylene blue. Biochim. Biophys. Acta **883,** 173, 1986.
34. Hollander, A.P., Heathfield, T.F., Webber, C., Iwata, Y., Bourne, R., Rorabeck, C., and Poole, A.R. Increased damage to type II collagen in osteoarthritic articular cartilage detected by a new immunoassay. J. Clin. Invest. **93,** 1722, 1994.
35. Kafienah, W., and Sims, T.J. Biochemical methods for the analysis of tissue-engineered cartilage. In: Hatton, P.V., and Hollander, A.P., eds. Biopolymer Methods in Tissue Engineering. Totowa, NJ: Humana Press, 2003, p. 217.
36. Malda, J., van Blitterswijk, C.A., Grojec, M., Martens, D.E., Tramper, J., and Riesle, J. Expansion of bovine chondrocytes on microcarriers enhances redifferentiation. Tissue Eng. **9,** 939, 2003.
37. Vunjak-Novakovic, G., Martin, I., Obradovic, B., Treppo, S., Grodzinsky, A.J., Langer, R., and Freed, L.E. Bioreactor cultivation conditions modulate the composition and mechanical properties of tissue-engineered cartilage. J. Orthop. Res. **17,** 130, 1999.
38. Nehrer, S., Breinan, H.A., Ramappa, A., Young, G., Shortkroff, S., Louie, L.K., Sledge, C.B., Yannas, I.V., and Spector, M. Matrix collagen type and pore size influence behaviour of seeded canine chondrocytes. Biomaterials **18,** 769, 1997.
39. Bhardwaj, T., Pilliar, R., Grynpas, M., and Kandel, R. Effect of material geometry on cartilaginous tissue formation *in vitro*. J. Biomed. Mater. Res. **57,** 190, 2001.
40. LiVecchi, A., Tombes, R., and Laberge, M. *In vitro* chondrocyte collagen deposition within porous HDPE: Substrate microstructure and wettability effects. J. Biomed. Mater. Res. **28,** 839, 1994.
41. Schulze-Tanzil, G., De, S.P., Villegas, C.H., John, T., Merker, H., Scheid, A., and Shakibaei, M. Redifferentiation of dedifferentiated human chondrocytes in high-density cultures. Cell Tissue Res. **308,** 371, 2002.
42. Solursh, M., and Meier, S. Effects of cell density on the expresion of differentiation by chick embryo chondrocytes. J. Exp. Zool. **187,** 311, 1974.
43. Gooch, K., Kwon, J., Blunk, T., Langer, R., Freed, L., and Vunjak-Novakovic, G. Effects of mixing intensity on tissue-engineered cartilage. Biotechnol. Bioeng. **72,** 402, 2001.
44. Hunziker, E.B., Driesang, I.M., and Saager, C. Structural barrier principle for growth factor-based articular cartilage repair. Clin. Orthop. **391,** S182, 2001.
45. Kandel, R., Boyle, J., Gibson, G., Cruz, T., and Speagle, M. *In vitro* formation of mineralized cartilagenous tissue by articular chondrocytes. In Vitro Cell. Dev. Biol. Anim. **33,** 174, 1997.
46. Broom, N.D., Oloyede, A., Flachsmann, R., and Hows, M. Dynamic fracture characteristics of the osteochondral junction undergoing shear deformation. Med. Eng. Phys. **18,** 396, 1996.

47. Woodfield, T.B.F., Miot, S., van Blitterswijk, C.A., Riesle, J. The regulation of expanded human nasal chondrocyte redifferentiation capacity by substrate composition and gas plasma surface modification. Biomaterials (in press).
48. Deschamps, A.A., Claase, M.B., Sleijster, W.J., de Bruijn, J.D., Grijpma, D.W., and Feijen, J. Design of segmented poly(ether ester) materials and structures for the tissue engineering of bone. J. Control. Release **78,** 175, 2002.
49. Bryant, S., and Anseth, K. Controlling the spatial distribution of ECM components in degradable PEG hydrogels for tissue engineering cartilage. J. Biomed. Mater. Res. **64,** 70, 2003.

Address reprint requests to:
Tim B.F. Woodfield, Ph.D.
Centre for Bioengineering, 5th Floor
Mechanical Engineering Building
University of Canterbury
Private Bag 4800
Christchurch 8020, New Zealand

E-mail: tim.woodfield@canterbury.ac.nz

This article has been cited by:

1. T. B. F. Woodfield, M. Guggenheim, B. von Rechenberg, J. Riesle, C. A. van Blitterswijk, V. Wedler. 2009. Rapid prototyping of anatomically shaped, tissue-engineered implants for restoring congruent articulating surfaces in small joints. *Cell Proliferation* **42**:4, 485-497. [CrossRef]
2. Travis J. Klein , Jos Malda , Robert L. Sah , Dietmar W. Hutmacher . 2009. Tissue Engineering of Articular Cartilage with Biomimetic ZonesTissue Engineering of Articular Cartilage with Biomimetic Zones. *Tissue Engineering Part B: Reviews* **15**:2, 143-157. [Abstract] [Full Text] [PDF] [PDF Plus]
3. James D. Kretlow, Simon Young, Leda Klouda, Mark Wong, Antonios G. Mikos. 2009. Injectable Biomaterials for Regenerating Complex Craniofacial Tissues. *Advanced Materials* NA-NA. [CrossRef]
4. Martin J Stoddart, Sibylle Grad, David Eglin, Mauro Alini. 2009. Cells and biomaterials in cartilage tissue engineering. *Regenerative Medicine* **4**:1, 81-98. [CrossRef]
5. Milind Singh , Cory Berkland , Michael S. Detamore . 2008. Strategies and Applications for Incorporating Physical and Chemical Signal Gradients in Tissue EngineeringStrategies and Applications for Incorporating Physical and Chemical Signal Gradients in Tissue Engineering. *Tissue Engineering Part B: Reviews* **14**:4, 341-366. [Abstract] [PDF] [PDF Plus]
6. Aurelio Salerno, Salvatore Iannace, Paolo A. Netti. 2008. Open-Pore Biodegradable Foams Prepared via Gas Foaming and Microparticulate Templating. *Macromolecular Bioscience* **8**:7, 655-664. [CrossRef]
7. Rouwayda El-Ayoubi , Nicoletta Eliopoulos , Robert Diraddo , Jacques Galipeau , Azizeh-Mitra Yousefi . 2008. Design and Fabrication of 3D Porous Scaffolds to Facilitate Cell-Based Gene TherapyDesign and Fabrication of 3D Porous Scaffolds to Facilitate Cell-Based Gene Therapy. *Tissue Engineering Part A* **14**:6, 1037-1048. [Abstract] [PDF] [PDF Plus]
8. Rouwayda El-Ayoubi, Nicoletta Eliopoulos, Robert Diraddo, Jacques Galipeau, Azizeh-Mitra Yousefi. 2008. Design and Fabrication of 3D Porous Scaffolds to Facilitate Cell-Based Gene Therapy. *Tissue Engineering Part A*, ahead of print080422095744451. [CrossRef]
9. L. Moroni, R. Schotel, D. Hamann, J.R. de Wijn, C.A. van Blitterswijk. 2008. 3D Fiber-Deposited Electrospun Integrated Scaffolds Enhance Cartilage Tissue Formation. *Advanced Functional Materials* **18**:1, 53-60. [CrossRef]
10. Anuj Tripathi, Neeraj Kathuria, Ashok Kumar. 2008. Elastic and macroporous agarose–gelatin cryogels with isotropic and anisotropic porosity for tissue engineering. *Journal of Biomedical Materials Research Part A* **9999A**, NA-NA. [CrossRef]
11. Jojanneke M. Jukes, Lorenzo Moroni, Clemens A. van Blitterswijk, Jan de Boer. 2008. Critical Steps toward a Tissue-Engineered Cartilage Implant Using Embryonic Stem Cells. *Tissue Engineering* **14**:1, 135-147. [CrossRef]
12. Jojanneke M. Jukes , Lorenzo Moroni , Clemens A. van Blitterswijk , Jan de Boer . 2008. Critical Steps toward a Tissue-Engineered Cartilage Implant Using Embryonic Stem CellsCritical Steps toward a Tissue-Engineered Cartilage Implant Using Embryonic Stem Cells. *Tissue Engineering Part A* **14**:1, 135-147. [Abstract] [PDF] [PDF Plus]
13. Lorenzo Moroni , Maurus Curti , Manfred Welti , Stephen Korom , Walter Weder , Joost R. de Wijn , Clemens A. van Blitterswijk . 2007. Anatomical 3D Fiber-Deposited Scaffolds for Tissue Engineering: Designing a NeotracheaAnatomical 3D Fiber-Deposited Scaffolds for Tissue Engineering: Designing a Neotrachea. *Tissue Engineering* **13**:10, 2483-2493. [Abstract] [PDF] [PDF Plus]
14. Natalja E. Fedorovich , Jacqueline Alblas , Joost R. de Wijn , Wim E. Hennink , Ab J. Verbout , Wouter J.A. Dhert . 2007. Hydrogels as Extracellular Matrices for Skeletal Tissue Engineering: State-of-the-Art and Novel Application in Organ PrintingHydrogels as Extracellular Matrices for Skeletal Tissue Engineering: State-of-the-Art and Novel Application in Organ Printing. *Tissue Engineering* **13**:8, 1905-1925. [Abstract] [PDF] [PDF Plus]
15. Azizeh-Mitra Yousefi, Chantal Gauvin, Louise Sun, Robert W. DiRaddo, Julio Fernandes. 2007. Design and fabrication of 3D-plotted polymeric scaffolds in functional tissue engineering. *Polymer Engineering & Science* **47**:5, 608-618. [CrossRef]
16. L. Moroni , J.A.A. Hendriks , R. Schotel , J.R. de Wijn , C.A. van Blitterswijk . 2007. Design of Biphasic Polymeric 3-Dimensional Fiber Deposited Scaffolds for Cartilage Tissue Engineering Applications. *Tissue Engineering* **13**:2, 361-371. [Abstract] [PDF] [PDF Plus]
17. L. Moroni, J.A.A. Hendriks, R. Schotel, J.R. De Wijn, C.A. Van Blitterswijk. 2007. Design of Biphasic Polymeric 3-Dimensional Fiber Deposited Scaffolds for Cartilage Tissue Engineering Applications. *Tissue Engineering*, ahead of print061220075423021. [CrossRef]
18. Joseph Jagur-Grodzinski. 2006. Polymers for tissue engineering, medical devices, and regenerative medicine. Concise general review of recent studies. *Polymers for Advanced Technologies* **17**:6, 395-418. [CrossRef]